Int. J. Heat Mass Transfer. Vol. 9, pp. 1401–1418. Pergamon Press 1966. Printed in Great Britain

TURBULENT TRANSPORT COEFFICIENTS IN SUPERSONIC FLOW†

JOHN H. MORGENTHALER‡ and JOSEPH M. MARCHELLO

Applied Physics Laboratory, The Johns Hopkins University, Silver Spring, Maryland, and University of Maryland, College Park, Maryland

(*Received* 14 *January* 1966)

Abstract—Hypersonic ramjets employing supersonic combustion of hydrogen fuel have attractive potentialities for future aircraft or launching systems. The object of the present work § was to study quantitatively the effects of fuel injection parameters on the mixing of gaseous hydrogen fuel with a supersonic air stream confined within a cylindrical duct, to provide some of the fundamental background needed for the design of supersonic combustors for high-performance engines. Hydrogen was injected at sonic velocities into Mach 2 and Mach 3 air streams, at overall equivalence ratios of 0·17 to 0·50, in both radial and axial (downstream) directions from circumferential wall slots. Results showed that considerably better mixing occurred in the case of radial injection, although the decrease in stagnation pressure also was greater for this case.

The eddy diffusivity of mass, E_d (turbulent diffusion coefficient) and radial velocity, $\bar{V}_r$, were determined by differentiating experimental concentration, velocity and density profiles, obtained at various axial distances from the injection station. For the radial injection case, with a 1-in i.d. test section, a simple model in which E_d varied only in the radial direction and $\bar{V}_r$ varied only in the axial direction, allowed reasonable correlation of the experimental results. The validity of the trends obtained in E_d and $\bar{V}_r$ were checked by numerical integration of the diffusion equation, and simultaneous solution of the diffusion and momentum equations; computed profiles agreed reasonably well with downstream experimental concentration and velocity profiles. A method for solving turbulent mixing problems by simultaneous solution of the diffusion, momentum and energy equations is presented.

NOMENCLATURE

a, arbitrary constant used to shift origin for Laurent series [ft];
c_p, specific heat at constant pressure [ft lb_f/lb_m deg R];
D, molecular diffusivity, or diffusion coefficient [ft^2/s];
E_d, eddy diffusivity of mass [ft^2/s];
E_m, eddy diffusivity of momentum [ft^2/s];
g_c, dimension constant [32·174 lb_m ft/lb_f s^2];
k_n, total mass flow rate within a stream tube (defined by equation 14) [lb_m/s];
Le_T, turbulent Lewis number, $\bar{\rho}E_d c_p/\varkappa$;
P, static pressure [lb_f/ft^2];
Pr_T, turbulent Prandtl number, $\bar{\rho}E_m c_p/\varkappa$;
r, radial coordinate [ft];
r^*, coordinate of wall or centerline (defined by equation 15) [ft];
r_s, radial coordinate of streamline [ft];
Sc_T, turbulent Schmidt number E_m/E_d;
V, mass-average or bulk velocity [ft/s];
Y, mass fraction hydrogen;
z, axial coordinate [ft];
ϵ, eddy viscosity [lb_m/ft s];
$\varkappa$, eddy thermal conductivity [ft lb_f/s ft degR];

† Presented at the Symposium on Fundamentals of Fluid Dynamics, 58th Annual Meeting of the American Institute of Chemical Engineers, Philadelphia, Pennsylvania, December 6–9, 1965.

‡ Present Address: General Applied Science Labs., Westbury, N.Y.

§ This work was sponsored by the Office of Aeronautical Research, Office of Advanced Research and Technology, National Aeronautics and Space Administration, Washington, D.C. The Applied Physics Laboratory operates under Contract NOw 62-064c with the Bureau of Naval Weapons, Department of the Navy.

μ, molecular shear viscosity [$lb_m/ft\ s$];
ρ, density [lb_m/ft^3].

Subscripts
r, radial component;
w, wall;
z, axial component.

Bars denote time-averaged, and primes fluctuating quantities

INTRODUCTION

HYPERSONIC ramjets with supersonic combustion diffusion flames and utilizing hydrogen fuel have attractive potentialities for future aircraft or launching systems. A basic understanding of the process in which fuel and air are mixed would be of great benefit in the design of a supersonic combustion chamber, and is the first step in the analysis of the combustion phenomenon. The problem of mixing fuel with a supersonic stream has been studied recently by a number of investigators [1–5]; generally, their work has been limited to the case of coaxial injection, neglecting both axial and radial gradients in static pressure. Because of the similarity of this geometry to the free jet geometry, the eddy viscosity, ϵ, was frequently assumed to be constant in the radial direction as has been experimentally substantiated for incompressible free jets [6, 7].

In this investigation, an effort was made to simulate the injection section of an actual combustion chamber, i.e. a ducted flow with axial pressure gradients. Since it is important to minimize strong disturbances in the flow in a supersonic combustion chamber (i.e. shock waves), injection of the fuel from the wall rather than from protruding wall injectors appeared desirable, as long as adequate mixing could be attained. In addition, protruding injectors would significantly increase structural problems. Because of its potential importance, injection from the wall was studied exclusively in this investigation in an effort to attain a quantitative understanding of this important injection geometry. Only cold flow mixing tests without combustion were conducted.

Injection from a wall slot can be in the axial direction parallel (downstream) to the direction of flow of the air stream, or in the radial direction perpendicular to the air stream, or at some intermediate angle. Since injection perpendicular and parallel to the air stream are the simplest of the practical geometries to treat analytically and provide bounds for the intermediate case of downstream injection at an angle to the flow, they were used exclusively in this investigation. Of course, coaxial injection has an important advantage over radial injection from the viewpoint of engine cycle performance because the downstream component of momentum of the injected fuel, even though it may be small, contributes to theoretical net engine thrust at hypersonic flight speeds. Also, radial injection would be expected to result in greater stagnation pressure losses.

Turbulent flow will occur in almost all practical supersonic combustion engines. Turbulent mixing is much more rapid, and hence more desirable than laminar mixing; therefore, it is important to understand the complex turbulent case. These flows are characterized by random fluctuations, so that it would appear logical to apply the methods of statistical mechanics to turbulent mixing problems. Unfortunately, the statistical theory of turbulence is not sufficiently developed to allow its application to the turbulent mixing problem considered herein, so that an alternative approach was required [7–9].

The phenomenological or semi-empirical approach which has been used successfully for a considerable period of time for investigating jet mixing problems [6–8, 10, 11] utilizes empirically determined turbulent transport coefficients. These eddy coefficients are:

(1) The eddy diffusivity of mass, E_d (turbulent diffusion coefficient).
(2) The eddy diffusivity of momentum, E_m (eddy kinematic viscosity).

(3) Eddy diffusivity of heat, or alternatively, the eddy thermal conductivity, $\varkappa$.

These coefficients must be experimentally determined because unlike their molecular counterparts, they are functions of (at least) the position in the flow field and the radial gradients of mass fraction, axial velocity, and temperature, respectively. Of course, they are applicable only for the particular experimental conditions investigated. They are useful for evaluating the degree of mixing obtained with a particular test geometry, and for comparing different geometries; however, their major contribution will be correlation of data obtained at the various flow conditions and injector sizes of interest in supersonic combustors, if such correlations are possible.

In this work the direct approach was chosen for the determination of turbulent transport coefficients, in which differentiated experimental data were used to evaluate each term in the equations of change, except for the coefficients. This approach was selected rather than the more usual one of assuming relationships to predict the coefficients, and then testing their validity by integrating the equations of change in an attempt to reproduce experimental profiles, because large variations in E_d and E_m were anticipated. Turbulent fluctuations do not exist in the laminar sublayer near the wall; therefore, molecular transport rather than turbulent eddy transport would be important in this region, and E_d and E_m both would approach zero. In the turbulent boundary layer, they would be relatively large compared to their molecular counterparts. In fact recent experimental investigations of supersonic mixing [5] have shown that even in the case of high-speed coaxial free jets, neither E_d, E_m, nor the eddy viscosity, $\epsilon = \bar{\rho}E_m$, is constant in the radial direction as often has been assumed.

In order to check the validity of the E_d's, E_m's and $\overline{V}_r$'s obtained, a numerical integration which used experimentally determined profiles as the initial conditions was used to solve the turbulent diffusion and momentum equations both separately and simultaneously. Inconsistencies in the eddy diffusivities caused by differentiation of the experimental data could be determined in this manner, and by using an iterative procedure, values could be continually improved.

BASIC EQUATIONS

The general equations of change for steady, axially symmetric, turbulent flow in which no significant variation in stagnation temperature occurs are summarized below [13]. Following standard notation, a bar is placed over symbols that represent time-averaged quantities.

Turbulent continuity equation

$$\frac{1}{r}\frac{\partial}{\partial r}(\overline{\rho V_r} r) + \frac{\partial}{\partial z}(\overline{\rho V_z}) = 0. \tag{1}$$

Turbulent diffusion equation

$$\overline{\rho V_r}\frac{\partial \overline{Y}}{\partial r} + \overline{\rho V_z}\frac{\partial \overline{Y}}{\partial z} = \frac{1}{r}\frac{\partial}{\partial r}\left[\bar{\rho}(D + E_{d_1}) r \frac{\partial \overline{Y}}{\partial r}\right] + \frac{\partial}{\partial z}\left[\bar{\rho}(D + E_{d_2})\frac{\partial \overline{Y}}{\partial z}\right]. \tag{2}$$

Turbulent Navier–Stokes momentum equations

$$\overline{\rho V_r}\frac{\partial \overline{V}_r}{\partial r} + \overline{\rho V_z}\frac{\partial \overline{V}_r}{\partial z} = -g_c\frac{\partial \bar{P}}{\partial r} + \frac{2\mu}{r}\left(\frac{\partial \overline{V}_r}{\partial r} - \frac{\overline{V}_r}{r}\right) + \frac{2\epsilon_1}{3r}\left(2\frac{\partial \overline{V}_r}{\partial r} - \frac{\overline{V}_r}{r} - \frac{\partial \overline{V}_z}{\partial z}\right) + \frac{\partial}{\partial r}\left[\frac{2(\mu + \epsilon_1)}{3}\left(2\frac{\partial \overline{V}_r}{\partial r} - \frac{\overline{V}_r}{r} - \frac{\partial \overline{V}_z}{\partial z}\right)\right] + \frac{\partial}{\partial z}\left[(\mu + \epsilon_2)\left(\frac{\partial \overline{V}_z}{\partial r} + \frac{\partial \overline{V}_r}{\partial z}\right)\right]. \tag{3}$$

$$\overline{\rho V_r}\frac{\partial \overline{V}_z}{\partial r} + \overline{\rho V_z}\frac{\partial \overline{V}_z}{\partial z} = -g_c\frac{\partial \bar{P}}{\partial z} + \frac{1}{r}\frac{\partial}{\partial r}\left[(\mu + \epsilon_3) r\left(\frac{\partial \overline{V}_z}{\partial r} + \frac{\partial \overline{V}_r}{\partial z}\right)\right] + \frac{\partial}{\partial z}\left[\frac{2(\mu + \epsilon_4)}{3}\left(2\frac{\partial \overline{V}_z}{\partial z} - \frac{\partial \overline{V}_r}{\partial r} - \frac{\overline{V}_r}{r}\right)\right] \tag{4}$$

† A constant stagnation temperature is a solution to the turbulent energy equation when turbulent Prandtl and Lewis numbers are unity [12].

where the turbulent transport coefficients are defined in such a manner that the laminar form of the equations is preserved

$$\overline{(\rho V_r)'Y'} \equiv -\bar{\rho}E_{d_1}\frac{\partial \bar{Y}}{\partial r} \tag{5}$$

$$\overline{(\rho V_z)'Y'} \equiv -\bar{\rho}E_{d_2}\frac{\partial \bar{Y}}{\partial z} \tag{6}\dagger$$

$$\overline{(\rho V_r)'V_r} \equiv -\frac{2\epsilon_1}{3}\left(2\frac{\partial \bar{V}_r}{\partial r} - \frac{\bar{V}_r}{r} - \frac{\partial \bar{V}_z}{\partial z}\right) \tag{7}$$

$$\overline{(\rho V_z)'V_r} \equiv -\epsilon_2\left(\frac{\partial \bar{V}_z}{\partial r} + \frac{\partial \bar{V}_r}{\partial z}\right) \tag{8}$$

$$\overline{(\rho V_r)'V_z} \equiv -\epsilon_3\left(\frac{\partial \bar{V}_z}{\partial r} + \frac{\partial \bar{V}_r}{\partial z}\right) \tag{9}$$

$$\overline{(\rho V_z)'V_z} \equiv -\frac{2\epsilon_4}{3}\left(2\frac{\partial \bar{V}_z}{\partial z} - \frac{\bar{V}_r}{r} - \frac{\partial \bar{V}_r}{\partial r}\right). \tag{10}$$

Equations (2) to (4) cannot be solved directly for the six unknown transport coefficients unless some assumptions are made concerning their relationships, e.g. that some are either equal or negligible. However, even when such assumptions are made, accurate determination of some of the remaining terms in these equations would be difficult using experimental data. An alternative approach, which leads to considerable simplification, is to make several general assumptions concerning the flow. The simplifying assumptions that appear reasonable for high-speed turbulent flow because of the importance of axially-directed convective bulk flow are:

(1) Diffusion in the axial direction is negligible compared to that in the radial direction.
(2) Viscous normal stresses are negligible compared to the pressure.
(3) Viscous shear stresses depend primarily on the radial gradient of axial velocity

$$(\partial \bar{V}_z/\partial r \gg \partial \bar{V}_r/\partial z).$$

(4) Fluctuating components of the axial velocity are negligible compared to corresponding time-average quantities

$$[\overline{\rho V_z V_z} \gg \overline{(\rho V_z)'V_z'}].$$

Assumption (2) appears reasonable because an order of magnitude analysis shows that viscous normal stresses are negligible compared to the pressure even in the boundary layer where viscous forces attain their maxima.

Using these assumptions, equations (2) and (4) become respectively

$$\overline{\rho V_r}\frac{\partial \bar{Y}}{\partial r} + \overline{\rho V_z}\frac{\partial \bar{Y}}{\partial z} = \frac{1}{r}\frac{\partial}{\partial r}\left[\bar{\rho}E_d r\frac{\partial \bar{Y}}{\partial r}\right] \text{and} \tag{11}$$

$$\overline{\rho V_r}\frac{\partial \bar{V}_z}{\partial r} + \overline{\rho V_z}\frac{\partial \bar{V}_z}{\partial z} = \frac{1}{r}\frac{\partial}{\partial r}\left[\bar{\rho}E_m r\frac{\partial \bar{V}_z}{\partial r}\right] - g_c\frac{\partial \bar{P}}{\partial z} \tag{12}$$

where $E_d \equiv E_{d_1}$ and E_m is defined by the relation

$$\overline{(\rho V_r)'V_z'} = -\bar{\rho}E_m\frac{\partial \bar{V}_z}{\partial r} \approx -\epsilon_3\frac{\partial \bar{V}_z}{\partial r}. \tag{13}$$

In equations (11) and (12) molecular transport has been neglected compared to turbulent transport, an assumption normally valid except within the laminar sublayer; however, they may still be applied within this region if E_d and E_m are considered the sum of the molecular plus turbulent coefficients.

Probably none of the terms in equation (3), the radial momentum equation, are large; therefore, it is difficult to conclude which, if any, of them may be neglected. Since the transfer of axial momentum is generally of greater interest than the transfer of radial momentum, frequently this equation need not be considered. However, if $\epsilon_2 \approx \epsilon_3$, i.e. $\overline{V_r}\,\overline{\rho' V_z'}$ and $\overline{V_z}\,\overline{\rho' V_z'}$ are small compared to $\bar{\rho}\,\overline{V_r' V_z'}$ (or are approximately equal), or if axial derivatives are much less than radial derivatives in this equation, ϵ_1 could be obtained. Alternatively, if $\overline{\rho V_r V_r} \gg \overline{(\rho V_r)'V_r'}$, ϵ_2 may be determined. If all the viscous terms in this equation are negligible, so that it reduces to an Euler equation, it still would be

† The axial dispersion coefficient is frequently defined in a similar manner to E_{d_2} [14].

useful for checking the consistency of the inertial and pressure terms, and hence, the experimental measurements.

DETERMINATION OF TURBULENT TRANSPORT COEFFICIENTS

One method for determining E_d, E_m and $\overline{V}_r$ is differentiation of the experimental concentration, velocity and density profiles, and substitution of these derivatives in equations (11) and (12). Using an assumed value of the turbulent Schmidt number, Sc_T (near unity), these equations can be solved simultaneously for E_d and $\overline{V}_r$. Equation (1) would be used to check the consistency of values of $\overline{V}_r$. If equation (1) were not satisfied, a new Sc_T would be assumed and the procedure repeated. An obvious disadvantage of this method is the need to obtain second derivatives from experimental data, which requires extremely closely spaced accurate data points.

One integration of equations (1), (11) and (12) eliminates the need for obtaining second derivatives and allows determination of the unknown terms directly. This integration can be accomplished by an extension of Shipman's method [9] in which these equations are integrated once in the radial direction, between either the wall or the centerline and a "streamline", i.e. a line bounding a fixed mass flow, designated $r_s(n)$.

The value of $r_s(n)$ is found for various test section lengths and values of the constant k_n by a numerical evaluation of the integral

$$\int_{r^*}^{r_s(n)} \overline{\rho V_z}\, r\, \mathrm{d}r = k_n \tag{14}$$

where r^* designates either the wall or the centerline. The boundary conditions at r^* are

$$r^* = \begin{cases} r_w: & \overline{V}_z = 0, \quad \overline{V}_r = 0, \quad \dfrac{\partial \overline{Y}}{\partial r} = 0 \\ 0: & \overline{V}_r = 0, \quad \dfrac{\partial \overline{Y}}{\partial r} = 0, \quad \dfrac{\partial \overline{V}_z}{\partial r} = 0 \end{cases} \tag{15}$$

since no mass diffuses through the wall, the velocity at the wall is zero, and the centerline is an axis of symmetry. Equation (14) shows that there will be no net flux of mass across the streamline by convection, although both hydrogen and air cross the streamline by diffusion (equal masses in opposite directions).

Multiplying each term in equation (1) by $r\,\mathrm{d}r$, integrating from either the wall or the centerline to r_s, and applying the generalized Liebnitz formula for interchanging the order of differentiation and integration yields

$$[\overline{\rho V_r} r_s]_{r_s} + \frac{\partial}{\partial z}\int_{r^*}^{r_s} \overline{\rho V_z}\, r\, \mathrm{d}r = \left[\overline{\rho V_z} r_s \frac{\partial r_s}{\partial z}\right]_{r_s}. \tag{16}$$

But equation (14) requires that the second term on the left be zero, so that at r_s

$$\overline{\rho V_r} = \overline{\rho V_z}\frac{\partial r_s}{\partial z}. \tag{17}$$

Equations (11) and (12) may be integrated in a similar manner using equations (15) and (17), to give

$$\frac{\partial}{\partial z}\int_{r^*}^{r_s} \overline{\rho V_z}\, \overline{Y} r\, \mathrm{d}r = \left[\bar{\rho} E_d r_s \frac{\partial \overline{Y}}{\partial r}\right]_{r_s} \tag{18}$$

$$\frac{\partial}{\partial z}\int_{r^*}^{r_s} \overline{\rho V_z}\, \overline{V}_z\, r\, \mathrm{d}r = \left[\bar{\rho} E_m r \frac{\partial \overline{V}_z}{\partial r}\right]_{r^*}^{r_s} - g_c \int_{r^*}^{r_s} \frac{\partial \overline{P}}{\partial z} r\, \mathrm{d}r. \tag{19}$$

These integral equations also can be obtained directly by noting that since neither hydrogen nor momentum leave or enter a stream tube by convection, any variation of these parameters within the stream tube must be caused by diffusion normal to the flow. Equations (18) and (19) were solved for E_d and E_m, respectively. Note that since $\partial \overline{V}_z/\partial r = 0$ at the centerline, no momentum flux crosses the centerline, but that there is a momentum flux to the wall since $\partial \overline{V}_z/\partial r \neq 0$ at the wall. As previously noted, near the wall in the laminar sublayer the molecular diffusivity and viscosity, D and μ, rather than E_d and E_m become important.

The integrals in equations (18) and (19) were

evaluated numerically at each test section length using interpolated concentration, velocity and density data, and the trapezoidal rule at intervals of 0·002 in; their axial variations were determined by fitting a truncated Laurent polynomial in $1/(z + a)$ and differentiating the polynomial. The terms $\partial\overline{Y}/\partial r$ and $\partial\overline{V}_z/\partial r$ were determined by numerical differentiation of the interpolated concentration and velocity data, using a five-point, second-order, running-smoothing routine and $\bar{\rho}$ was determined by interpolation of the density profiles. If radial pressure variations can be experimentally determined, the last term in equation (19) may be evaluated numerically using the measured local free-stream static pressure, e.g. obtained with a conical probe. This numerical evaluation could be most readily accomplished using the Liebnitz formula

$$\int_{r^*}^{r_s} \frac{\partial \bar{P}}{\partial z} r\,dr = \frac{\partial}{\partial z}\int_{r^*}^{r_s} \bar{P} r\,dr - \left[Pr_s \frac{\partial r_s}{\partial z}\right]_{r_s}. \quad (20)$$

Since r^* may equal either 0 or r_w, the various integrations may be carried out either from the wall or the centerline, so that two values of E_d and E_m may be obtained. These values will agree only if mass and momentum balances are consistent.

No effort was made to determine the eddy diffusivity of heat, or eddy thermal conductivity in this work since the stagnation temperature remained approximately constant throughout the flow; however, the simplified [12] energy equation also can be integrated in a similar manner and used to determine these parameters when stagnation temperature measurements are available [13]. In this way the turbulent Prandtl and Lewis numbers can be obtained as well as the turbulent Schmidt number.

APPARATUS

The apparatus used for these mixing studies is shown schematically in Fig. 1. Details of the self-aligning, stainless steel test sections are shown in Fig. 2. The supersonic air flow was created with contoured, axially symmetric, Mach 2 and Mach 3 Clippinger-type nozzles [15], which were designed by the method of characteristics, with sharp edges at their sonic plane surfaces; exit diameters were 1·000 in. Boundary-layer thickness for the Mach 2 nozzle at the injection station, computed from the von Kármán momentum relation was approximately 0·02 in. The nozzles were calibrated so they could meter the air flow.

Air flow rate was sufficient so that test section static pressures were maintained above atmospheric in all runs and no ambient air could enter the test section through the subsonic portion of the boundary layer.

Hydrogen was metered with a 0·079-in sonic venturi and injected from a ring manifold through the circumferential slots into the supersonic air stream (Fig. 2). The manifold pressure was normally considerably greater than twice the test section pressure. The hydrogen attained sonic velocity just prior to its initial contact with the air; no effort was made to balance the injection pressure and test section static pressure by varying the width of the slot, as slot width was considered an independent variable. Because the hydrogen expanded from a higher pressure into the air stream, a momentary supersonic hydrogen flow probably was established which initially was thought would enhance the penetration, and hence the mixing. Fortunately, detailed consideration of the complex injection process was not required in the analysis.

Variation in composition between free-stream and sampling system caused by chemical reactions in the probe did not have to be considered since no combustion occurred. Confirmation that true samples of the free stream were obtained with the 0·010-in i.d. capillary probes was achieved in the Mach 2 tests by mixing hydrogen with air in the subsonic air line about 15 ft upstream of the nozzle, so that the gases were completely mixed at the sampling position; radial transverses with the sampling probe

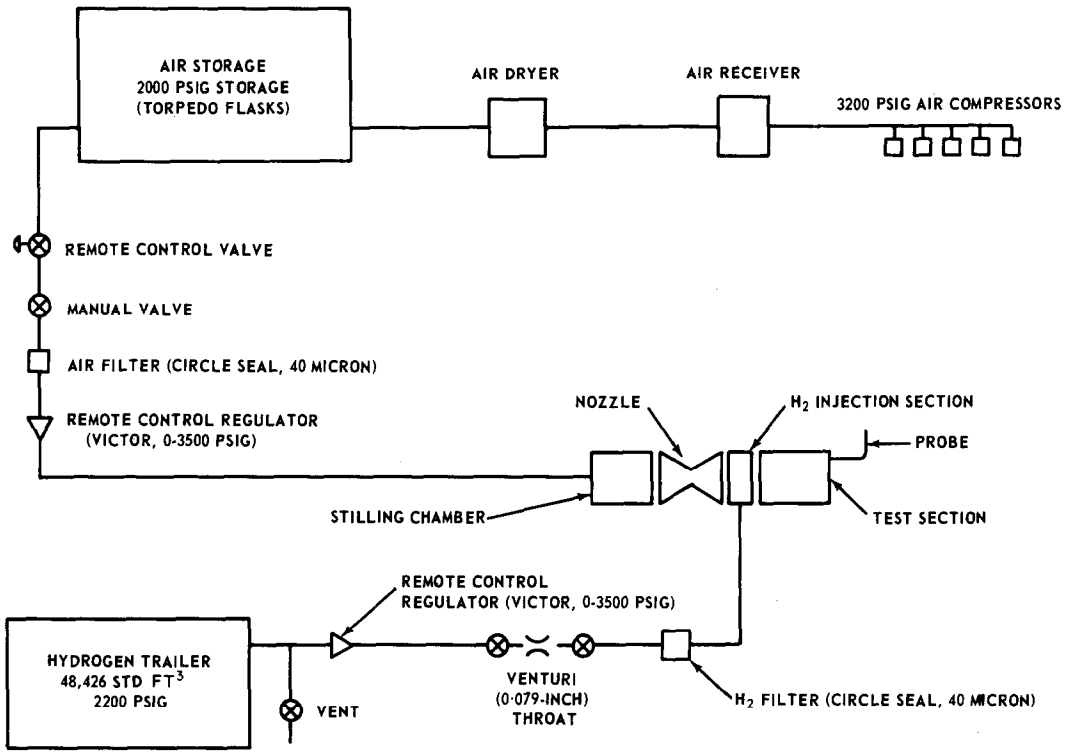

FIG. 1. Schematic diagram of apparatus.

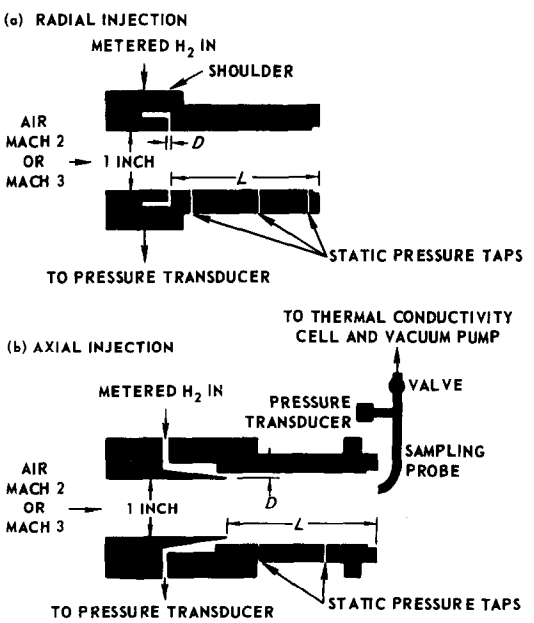

FIG. 2. Details of test sections.

confirmed that the mixing was complete. Agreement between concentrations computed from the metering systems was normally within a few per cent of that obtained with the calibrated thermal conductivity cell. Therefore, separation of hydrogen and air did not appear to be a problem [16, 17]. Special problems prevented a complete investigation of Mach 3 air flows.

PROCEDURE

Considerable care was taken during each run to maintain constant flow rates of hydrogen and air, since approximately 30 min (30–40 data points) was required to complete each set of radial profiles. A combination milling and rotary table was used to traverse the sampling probe. At each sampling point, the position of the probe with which hydrogen concentration and pitot (ram) pressure were sequentially obtained, was visually determined with a dial

micrometer. The dial was initially adjusted when the probe made contact with the wall lighting a flashlight. The probe tip was positioned 0·1 in upstream of the exit plane, so that the wall static pressure at the sampling station could be accurately determined.

A VECO M 182, open-diffusion, thermal conductivity gas analysis cell was used to determine hydrogen concentrations. It was calibrated with known mixtures of hydrogen and air each run day. Cell pressure was manually adjusted using a mercury manometer and a stable reading obtained on a strip-chart recorded prior to recording each data point on magnetic tape. Cell temperatures were controlled by immersing the waterproofed cell in an ice bath contained in a large Dewar flask. Immediately after recording the concentration, the sampling system was isolated from the probe and pressure transducer (Fig. 2), and the pitot pressure recorded in a similar manner.

The stagnation temperature of the hydrogen and air was measured just prior to injection; both were approximately equal to the ambient storage temperature. In a few cases experimental stagnation temperature profiles were obtained with a shielded thermocouple probe. Typical results [13] showed the maximum radial variation to be only about 3 per cent; therefore, in the data reduction the simplifying assumption was made that the stagnation temperature remained constant and equal to the mass-average stagnation temperature of the hydrogen and air.

In most Mach 2 runs, a cone-static pressure probe was used in an attempt to determine local free-stream static pressures. Unfortunately, Mach number profiles computed for identical flow conditions, but different test section lengths, were irregular and inconsistent, even when a probe with a 10-degree semivertex angle and a 0·014-in i.d. pressure tap, 0·16 in from the tip was used. Mach number profiles also were computed using measured wall static pressures assuming no radial pressure variation, although clearly radial pressure variations caused by the hydrogen injection occurred in the flow, especially near the injection station. These profiles appeared more reasonable than those computed using cone static pressures. Since a great deal of additional effort would have been required to obtain satisfactory local static pressures, data were reduced using measured wall static pressures, and assuming radial pressure variations to be negligible.

In the boundary layer where the flow was subsonic, the Mach number was computed from the appropriate relation for adiabatic flow of a perfect gas; when the flow was supersonic, the Mach number was computed from the Rayleigh pitot formula. Calculations were somewhat simplified because the specific heat ratio, γ, is independent of the hydrogen air composition for the conditions considered, and equal to 1·4. The static temperature was computed from the Mach number assuming the stagnation temperature remained constant. The density was computed using the perfect gas law, and the axial velocity from the Mach number and the speed of sound. Details of these computations are given in reference [13].

The magnetic data tape taken during each run was reduced on an IBM 7094 computer. All information needed for subsequent data reduction or plotting was punched on IBM cards to minimize the opportunity for error and facilitate handling the mass of data.

EXPERIMENTAL RESULTS

A series of runs with sonic (3900 ft/s) radial hydrogen injection was completed with 1·06 lb/s Mach 2 air and 0·005, 0·010 and 0·015 lb/s hydrogen (overall equivalence ratios of 0·17, 0·33 and 0·50, respectively) for an injection slot width of 0·005 in. Concentration, velocity, density and Mach number profiles were obtained for up to 5 different test section lengths. A set of typical profiles, obtained for an injection rate of 0·005 lb/s are presented in Figs. 3–6. The run conditions and instrumentation details are presented in reference [13].

Some justification for using the simplifying assumption that the static pressure did not

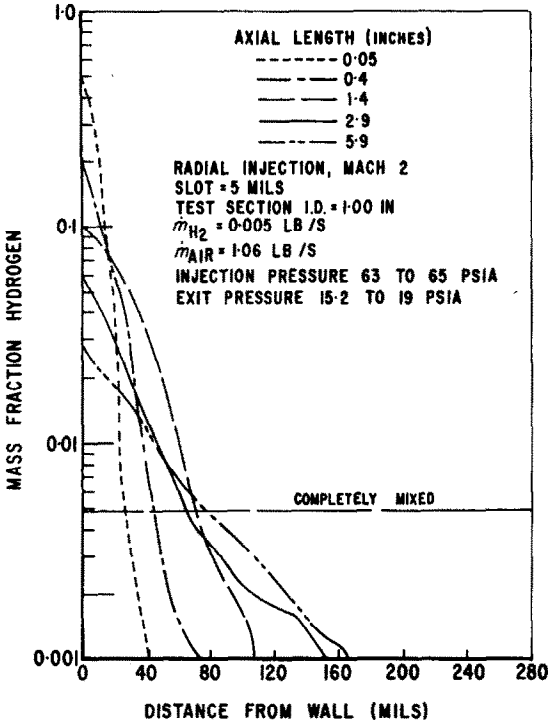

FIG. 3. Hydrogen concentration profiles, radial hydrogen injection, Mach 2 air.

vary greatly in the radial direction was obtained from the computed mass and momentum balances. Air mass balances normally agreed within a few per cent; hydrogen balances generally were low by 12 to 30 per cent. Lack of agreement of the hydrogen balances is believed to have been caused by the difficulty in accurately determining the velocity and density, particularly in the region near the wall where hydrogen concentration was large. Momentum balances were consistent and appeared reasonable since the momentum should decrease gradually with axial length (because of wall friction), and radial hydrogen injection rate (because of mass addition).

For clarity, curves are drawn in the figures; the original data points are presented in reference [13]. Because of very large variation of concentration with length, the hydrogen concentration profiles in Fig. 3 are plotted on a logarithmic scale as mass fraction hydrogen; hydrogen mass fractions of 0·10 and 0·40 are equivalent to 62 and 91 mole per cent, respectively. Since no hydrogen penetrates the wall, the slope of the concentration profiles should be zero at the wall; however, the finite probe size did not permit this boundary condition to be confirmed experimentally. The expected trends of decreasing hydrogen concentration with both radial distance from the wall and axial length were obtained. Several local irregularities occurred which may have been caused by a slight amount of play in the probe transversing mechanism. A stationary sampling rake might eliminate this problem in future experiments.

Velocity profiles for the short test section lengths reached their maxima near the wall as shown in Fig. 4. This effect probably was caused by initial supersonic expansion of hydrogen from the injection slot into the lower static pressure environment of the test section. The irregularities in these profiles were probably caused by oblique shock waves which decreased in strength with distance from the injection slot. In the region near the wall velocity decreased with test section length as expected for a developing boundary layer. As anticipated, the error introduced by assuming that no radial static pressure variation occurred was most significant for the 0·05-in length.

In the region near the wall, densities presented in Fig. 5 increased with test section length corresponding to the decrease in hydrogen concentration as mixing proceeds. The fact that the density profiles exhibit more irregularity than either the concentration or velocity profiles is not surprising since they depend on the same measurements as the velocity, in addition to the static pressure directly.

The Mach number profiles are presented in Fig. 6. The fact that, except for the 0·05-in length, they decreased with axial length, and were generally parallel, was further support for use of the wall static pressures in the Mach number computation. Except for axial stations close to the injection station, radial variations in

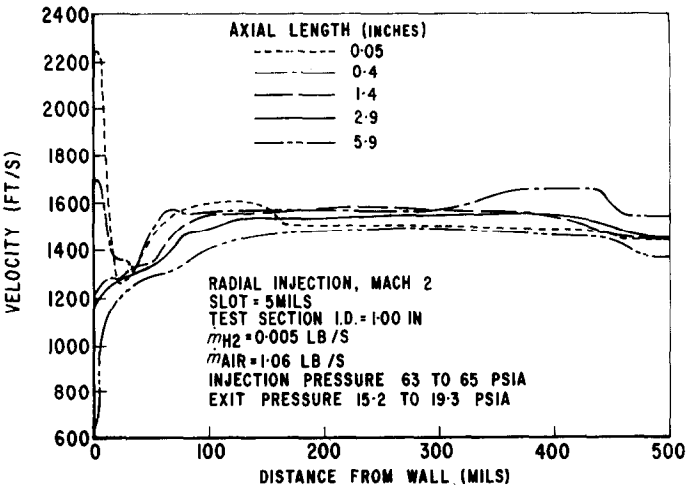

FIG. 4. Velocity profiles, radial hydrogen injection, Mach 2 air.

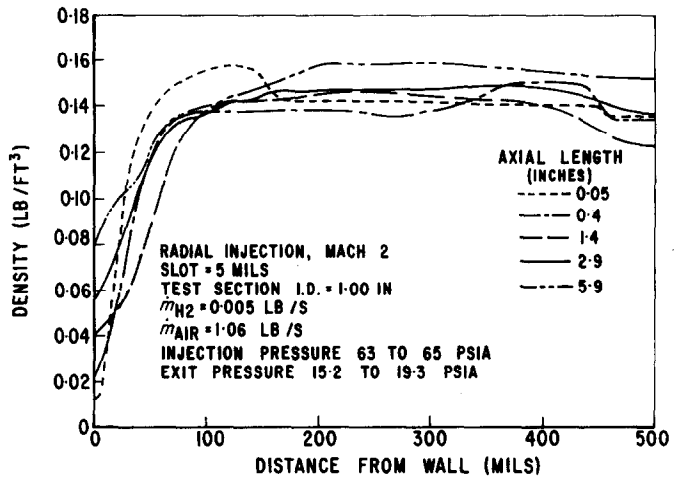

FIG. 5. Density profiles, radial hydrogen injection, Mach 2 air.

pressure may not have been very significant. The average Mach number in Fig. 6 is about 1·8; corresponding averages for hydrogen injection rates of 0·010 and 0·015 lb/s were 1·4 and 1·2, respectively. In a constant area duct, hydrogen injection rates producing overall equivalence ratios significantly greater than 0·5 would result in subsonic flow over a large portion of the flow field; therefore, an expanding combustor geometry, e.g. conical, must be employed in order to prevent choking the flow.

Hydrogen concentration profiles for sonic radial injection rates of 0·010 and 0·015 lb/s into a 1·06 lb/s, Mach 2 air stream are presented in Figs. 7 and 8. The corresponding velocity, density, Mach number, and static temperature profiles are presented in reference [13]. Because of the limited penetration at the low flow rates, an expanded abscissa was used in Fig. 3. Comparison of Figs. 3, 7 and 8, shows that increasing the hydrogen injection rate does not result in significantly increased maximum

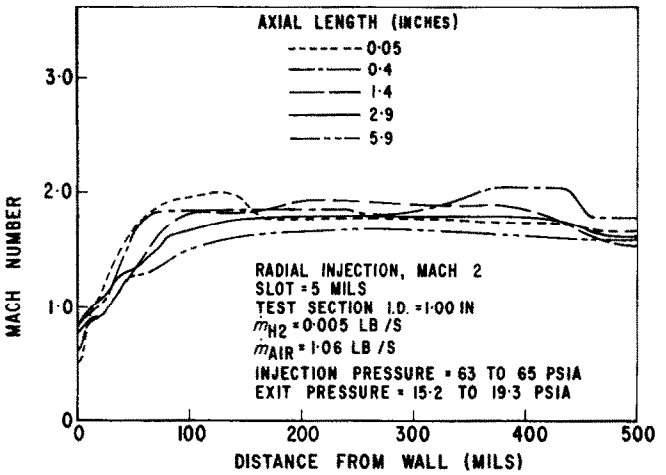

FIG. 6. Mach number profiles, radial hydrogen injection, Mach 2 air.

(wall) hydrogen concentrations, and frequently results in *lower* wall concentrations. Penetration and spreading is greatly enhanced at the higher injection rates; however, stagnation pressure losses also are greater.

Runs also were made with 1·99 lb/s Mach 3 air and sonic radial hydrogen injection rate of 0·009 lb/s for an injection slot width of 0·005 in. A higher air flow rate was required in the Mach 3 tests than the Mach 2 test in order to

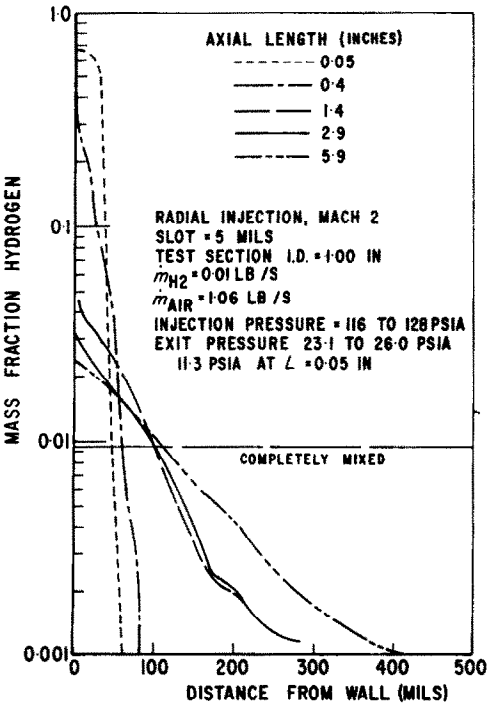

FIG. 7. Hydrogen concentration profiles, radial hydrogen injection, Mach 2 air.

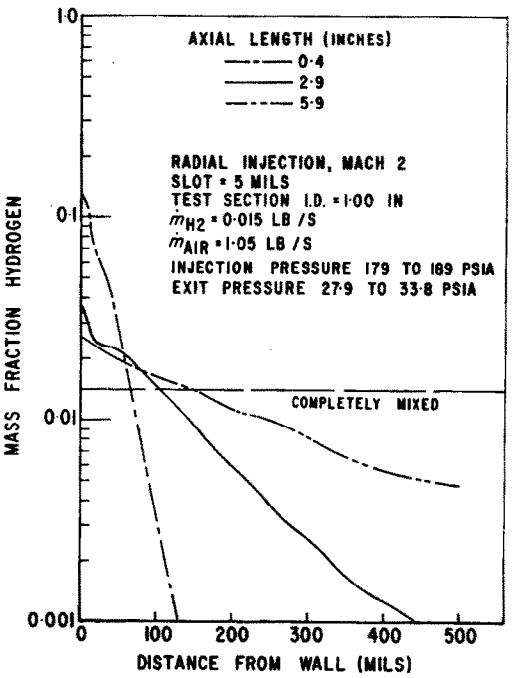

FIG. 8. Hydrogen concentration profiles, radial hydrogen injection, Mach 2 air.

maintain test section static pressures greater than ambient. Unfortunately only two sets of profiles at different test section lengths were obtained with the self-aligning, stainless steel sections. In order to obtain any quantitative results, preliminary data obtained with somewhat oversized brass test sections, and in some cases slightly different hydrogen and air flow rates had to be used. Because of various experimental problems, the Mach 3 data presented in Fig. 9 were smoothed before differentiating them [13]. The original data are presented in reference [13].

Early in the test program a series of runs was made with brass test sections in a preliminary investigation of the relative merits of the axial as opposed to radial injection. Test section geometries investigated were illustrated in Fig. 2. In Fig. 10 hydrogen concentration profiles for axial injection are presented. Comparison of these results with those of Figs. 3, 7 and 8 indicate that for these conditions, radial injection

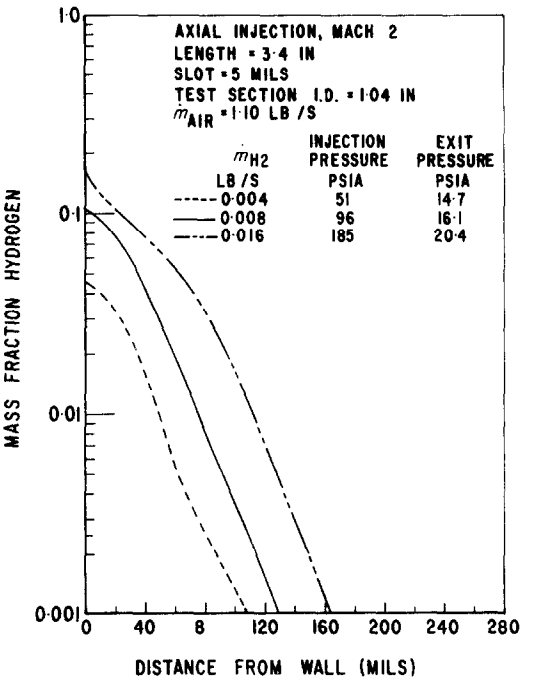

FIG. 10. Hydrogen concentration profiles, axial hydrogen injection, Mach 2 air.

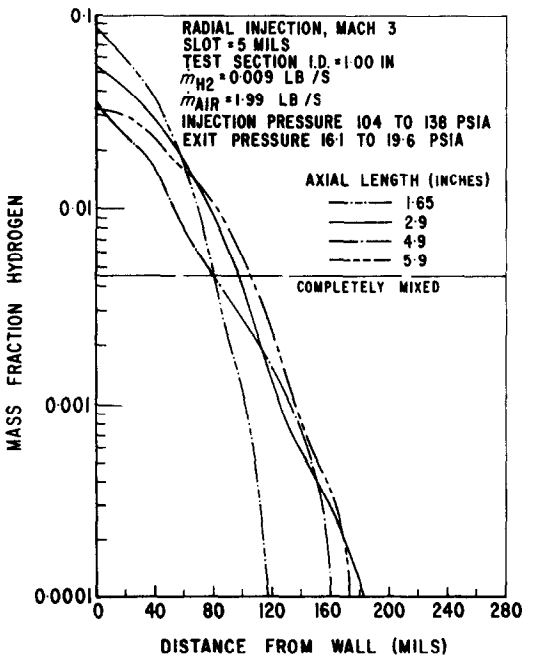

FIG. 9. Hydrogen concentration profiles, radial hydrogen injection, Mach 3 air.

is definitely superior to axial injection both from the standpoint of wall concentrations and depth of penetration. Thus the major experimental effort in this investigation was directed toward radial injection.

DETERMINATION OF E_d AND V_r

Experimental profiles were used to compute E_d and $\bar{V}_r$ using the procedure previously discussed. In obtaining $\bar{V}_r$ the assumption was made that $\overline{\rho' V_r'}$ and $\overline{\rho' V_z'}$ were negligible compared to $\bar{\rho}\bar{V}_r$ and $\bar{\rho}\bar{V}_z$ respectively. Results for 0·005 lb/s radial hydrogen injection into 1·06 lb/s Mach 2 air (Figs. 3–6) are presented in Table 1. Considerable variation occurred in E_d and $\bar{V}_r$ in both the radial and axial directions, which was not unexpected because of the simplifying assumptions made in reducing the data, i.e. that no radial static pressure variations occurred. The negative value obtained at the 0·4-in length undoubtedly results from the difficulty in obtaining axial variations from only a few widely

Table 1. Eddy diffusivity of mass and radial velocity, radial hydrogen injection, Mach 2 air

(Injection slot = 0·005 in; Test section i.d. = 1·00 in; $\dot{m}_{H_2}$ = 0·005 lb/s; $\dot{m}_{Air}$ = 1·06 lb/s)

Distance from wall x (mils)	Axial length (in.)			
	0·4	1·4	2·9	5·9
	(a) Eddy diffusivity of mass (ft^2/s)			
5	0·009	0·017	0·007	0·001
10	0·011	0·023	0·012	0·007
15	0·016	0·030	0·013	0·018
20	0·024	0·034	0·017	0·031
25	0·026	0·034	0·022	0·040
30	0·018	0·031	0·027	0·046
35	0·020	0·028	0·032	0·049
40	0·026	0·025	0·042	0·051
50	0·033	0·024	0·070	0·064
70	−0·046	0·046	0·139	0·137
100	0	0·146	0·316	0·245
	(b) Radial velocity (ft/s)			
5	2·57	0·97	0·48	0·04
10	3·63	1·68	1·12	0·51
15	3·68	2·13	1·80	1·20
20	3·17	2·41	2·43	1·86
25	2·58	2·61	2·94	2·45
30	1·64	2·72	3·31	2·92
35	0·33	2·69	3·59	3·31
40	−1·28	2·52	3·76	3·61
50	−5·35	1·84	3·74	3·94
70	−11·30	−0·14	3·22	3·88
100	−13·51	−2·48	2·24	3·53

spaced test section lengths, and especially the difficulty in obtaining the proper slopes at the end points. At relatively large distances from the wall where the concentration profiles approach zero, an unreal increase in E_d always occurred; of course, this result was ignored in establishing trends [12]. In spite of the fact that the largest radial pressure variations undoubtedly occurred with the 0·05-in test section, results obtained with it generally supported the trends obtained with the other lengths [13]. Valid E_m's could not be obtained from the velocity data because the differentiated velocity profiles were even less accurate than the original velocity data, and considerably more variation occurred in E_m than in E_d. However, despite the variation in E_d and $\bar{V}_r$, which in some cases resulted in physically unreal negative E_d's, general trends in both E_d and $\bar{V}_r$ occurred, which were consistent for all the data obtained. Although clearly an oversimplification, the trends suggested a very simple model, which proved surprisingly useful, i.e. E_d varies only in the radial direction and $\bar{V}_r$ varies only in the axial direction.

Although $\bar{V}_r$ appeared to depend primarily on axial length, the radial distance over which results could be checked by integration of the diffusion equation was not great because of the limited hydrogen penetration. Since $\bar{V}_r$ must be zero at the wall because of the no-slip condition and also at the centerline because of symmetry, in general it also must depend on radial position. However, ignoring this dependence over the region within 0·1 in of the wall appeared to be a reasonable first approximation. More exact data and profiles for additional intermediate test section lengths are required for accurate determination of the detailed radial and axial variation of the turbulent transport coefficients. In the absence of such data, it was important to determine the validity of the simple model by integrating the basic equations. Of course, agreement between computed and experimental profiles merely demonstrated the consistency of the eddy coefficients and the original profiles. Nothing concerning their absolute correctness was proven; results can be no better than the original experimental data.

A summary of the best values of E_d and $\bar{V}_r$ obtained using the simple model is given in Figs. 11 and 12. For Mach 2 air the maximum value of E_d increased almost an order of magnitude by doubling the hydrogen injection rate from 0·005 to 0·010 lb/s. However, a further increase in hydrogen flow rate to 0·015 lb/s increased E_d only 30 per cent above that for the 0·010 lb/s rate. The effect of hydrogen injection rate on E_d suggests that for these Mach 2 test conditions, a critical turbulence level is reached at a radial hydrogen injection rate between 0·005 and 0·010 lb/s. Determination of

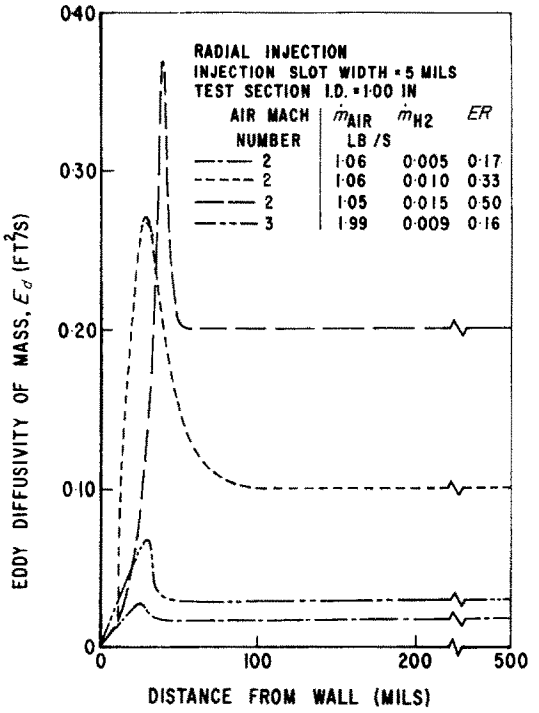

FIG. 11. Radial variation of eddy diffusivity of mass.

this critical level would be very important in the design of practical combustors. Values of E_d plotted for distances greater than 0·2 in from the wall were estimated by extrapolation because of the limited penetration at the shorter test section lengths.

Values of E_d and $\bar{V}_r$ for Mach 3 air at 1·99 lb/s and a hydrogen injection rate of 0·009 lb/s are very similar to those obtained for Mach 2 air at 1·06 lb/s and a hydrogen injection rate of 0·005 lb/s, which suggests that at the same overall hydrogen/air ratio, the inlet Mach number does not greatly affect E_d. This indication that E_d depends primarily on the *overall ratio* of hydrogen/air, rather than on actual flow rates of either constituent, or on the inlet Mach number, is very important; however, additional data are required to confirm this result.

For simplicity E_d used in this investigation was considered to be the sum of D, which was negligible throughout the flow field except in the immediate vicinity of the wall, *plus* E_d. At the experimental conditions $D = 0{\cdot}0006$ ft²/s. Diffusivities of this general magnitude were actually obtained from the experimental profiles within 0·002 in of the wall, and this value was used throughout as E_d at the wall. Since E_d and $\bar{\rho}$ both always reached minimum values at the wall, the model used by previous investigators [2, 4, 10] in which either $\bar{\rho}E_d$ or $\bar{\rho}^2E_d$ was assumed constant in the radial direction clearly does not apply for the case of wall injection of hydrogen into air.

The decrease in $\bar{V}_r$ with axial length shown in Fig. 12 was anticipated, since it should depend on the magnitude of the concentration gradients. Again results for Mach 2 and Mach 3 at the same overall equivalence ratio are very similar.

The magnitudes of E_d's presented in Fig. 11 are similar to those of other investigators despite the greatly different geometries and flow conditions investigated. Zakkay *et al.* [4] obtained values between 0·3 and 0·7 ft²/s in their supersonic, coaxial turbulent mixing studies. Values

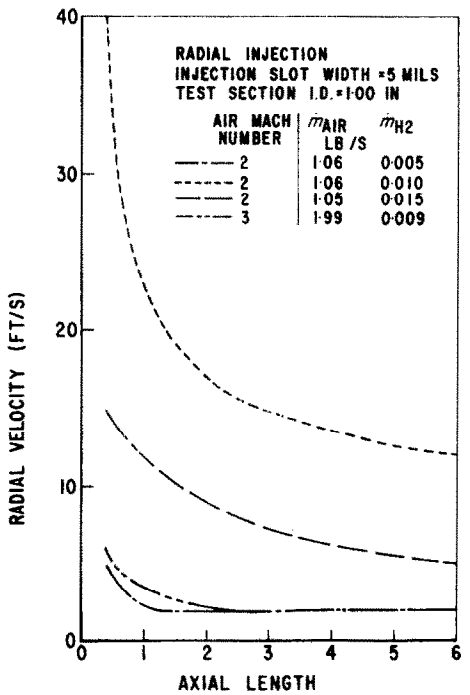

FIG. 12. Axial variation of radial velocity.

of 0·1–0·2 ft^2/s were obtained by Kingsland in his studies of diffusion in the wake of a circular cylinder at Mach 5·8 [18]. Longwell and Weiss [19] obtained values ranging from 0·3 to 0·6 ft^2/s, essentially independent of pressure, in their investigation of mixing of injected liquids in high-velocity subsonic air streams. These results suggest that the variation in E_d rather than its magnitude may be the significant effect to be obtained from future investigations.

SOLUTION OF DIFFUSION AND MOMENTUM EQUATIONS

Since the ultimate usefulness of the turbulent transport coefficients is the ability to predict concentration and velocity profiles, a numerical procedure (Crank–Nicolson) was developed for integrating the diffusion and momentum equations [13]. In the turbulent diffusion equation, the value of $\bar{V}_z$, $\bar{\rho}$ and $\partial\bar{\rho}/\partial r$ at any axial position were determined by fitting a polynomial in $1/(z + a)$ through experimental points obtained at various axial stations but at the same radial position. An iterative procedure was used in the solution of the momentum equation, since experimental values of $\bar{V}_z$ were not used in this case in which $\bar{V}_z$ was being computed.

Hydrogen concentration profiles obtained at various axial locations from numerical integrations of the diffusion equation, using the E_d and $\bar{V}_r$ profiles presented in Figs. 11 and 12, compared reasonably well with corresponding experimental profiles. Typical results are presented in Table 2. These results support the conclusion that the simple model used for representing E_d and $\bar{V}_r$, although obviously not exact, gives reasonable results throughout the mixing region investigated, and that the effect of the various parameters on E_d is reasonably established. Also, exact knowledge of the initial profiles does not appear critical for the numerical integration of the diffusion equation; the approximate velocity and density profiles obtained even for the 0·05-in length appear an adequate approximation. Much poorer agreement between computed and experimental profiles was obtained in some cases when only minor changes were made in E_d or $\bar{V}_r$ from those

Table 2. Comparison between experimental and computed concentration profiles radial hydrogen injection, Mach 2 air

(Injection slot = 0·005 in; Test section i.d. = 1·00 in; $\dot{m}_{H_2}$ = 0·005 lb/s; $\dot{m}_{Air}$ = 1·06 lb/s)

Distance from wall x (mils)	z = 0·4 in Initial profile Y_{exp}	z = 1·4 in		z = 2·9 in		z = 5·9 in	
		Y_{exp}	Y_{comp}	Y_{exp}	Y_{comp}	Y_{exp}	Y_{comp}
0	0·225	0·102	0·117	0·060	0·064	0·028	0·033
7·6	0·151	0·092	0·086	0·051	0·054	0·026	0·031
16·1	0·078	0·074	0·062	0·037	0·045	0·020	0·030
25·8	0·044	0·060	0·042	0·024	0·037	0·017	0·026
36·9	0·012	0·040	0·024	0·015	0·027	0·014	0·023
50·1	0·003	0·019	0·009	0·009	0·015	0·009	0·017
66·2	0·001	0·007	0·002	0·005	0·006	0·006	0·010
87·0	0	0·002	0	0·003	0·001	0·004	0·004
116·2	0	0	0	0·002	0	0·003	0·001
166·0	0	0	0	0	0	0·001	0
215·5	0	0	0	0	0	0	0
500·0	0	0	0	0	0	0	0
$\sum_i(\rho Y V_z A)_i$	0·0044	0·0050	0·0036	0·0039	0·0047	0·0034	0·0045
$\sum_i(\rho V_z A)_i$	1·056	1·014	0·9939	1·063	1·034	1·069	1·043

presented in Figs. 11 and 12 [13]. In the solutions of the momentum equation, better agreement was obtained between experimental and computed values of $\bar{V}_z$ when E_m was assumed equal to E_d (i.e. $Sc_T = 1$), than when values obtained directly from equation (19) were used.

SIMULTANEOUS SOLUTION OF DIFFUSION AND MOMENTUM EQUATIONS

The least satisfying aspect of separate solutions of the diffusion and momentum equations is the need to specify density profiles in advance, which require prior knowledge of both the composition and static temperature. Of course, the integration described above is the ultimate check of the consistency of the eddy diffusivity determinations. However, the need for specifying density profiles can be overcome by simultaneous solution of the diffusion and momentum equations using a numerical iterative procedure, provided the stagnation temperature is assumed constant throughout the flow, an assumption already made in the computation of the experimental density profiles. If radial pressure gradients occur in the flow, the integration is still possible as long as the detailed pressure variation is known. Since initial $\bar{Y}$ and $\bar{V}_z$ profiles are known, the static temperature can be computed. A density then can be computed using the known initial value of $\bar{Y}$, and the value of $\partial\bar{\rho}/\partial r$ can be obtained by numerical differentiation of this computed density profile. The diffusion and momentum equations now can be solved using these initial values of the density, its radial derivative, and the initial value of $\bar{V}_z$ for a first iteration to give new values of $\bar{Y}$ and $\bar{V}_z$ at the next axial station. Averaging the new and initial values gives an improved estimate of the true value of these terms midway between the new and initial values. New

Table 3. Comparison between experimental and computed velocity and concentration profiles radial hydrogen injection. Mach 3 air
(Injection slot = 0·0052 in; Test section i.d. = 1·00 in; $\dot{m}_{H_2}$ = 0·010 lb/s; $\dot{m}$ = 1·99 lb/s)

Distance from wall	z = 1·65 in Initial profile		z = 2·9 in Exp.		z = 2·9 in Computed		z = 5·9 in Exp.		z = 5·9 in Computed		Transport coefficients	
x (mils)	Y_{exp}	$V_{z_{exp}}$ (ft/s)	Y_{exp}	$V_{z_{exp}}$ (ft/s)	Y	V_z (ft/s)	Y_{exp}	$V_{z_{exp}}$ (ft/s)	Y	V_z (ft/s)	x (mils)	$E_d = E_m$ (ft²/s)
0	0·084	0	0·053	1117†	0·054	0	0·032	1043†	0·032	0†	0	0·0006
7·6	0·075	1450	0·051	1313	0·053	1122	0·031	1237	0·032	937	5	0·008
16·1	0·063	1511	0·046	1394	0·048	1372	0·029	1315	0·030	1171	10	0·017
25·8	0·054	1581	0·040	1461	0·043	1491	0·028	1405	0·029	1306	15	0·023
36·9	0·040	1638	0·032	1509	0·036	1574	0·024	1470	0·026	1417	20	0·030
50·1	0·026	1668	0·023	1591	0·025	1660	0·019	1533	0·021	1553	25	0·035
66·2	0·012	1735	0·014	1652	0·014	1747	0·014	1650	0·014	1680	30	0·040
87·0	0·003	1869	0·008	1768	0·005	1834	0·008	1738	0·008	1777	35	0·035
116·2	0	1908	0·002	1864	0·001	1890	0·003	1798	0·002	1843	40	0·030
166·0	0	1910	0	1921	0	1901	0	1882	0	1877	45	0·025
215·5	0	1925	0	1927	0	1914	0	1900	0	1890	50	0·025
500·0	0	1904	0	1840	0	1890	0	1881	0	1869	100	0·025
											300	0·025
$\sum_i(\rho Y V_z A)_i$	0·0088		0·0076		0·0074		0·0072		0·0071		500	0·025
$\sum_i(\rho V_z A)_i$	2·110		1·972		1·968		1·980		2·076		z (in)	V_r (ft/s)
$\sum_i(\rho V_z^2 A)_i$	123·6		114·7		117·6		112·4		121·6		1·4	3
											2·9	2
											5·9	2

† The velocity at the wall was set to zero for the initial profile because of the boundary condition; experimental values were never zero because of the finite probe size.

values of $\overline{V}_z$, $\bar{\rho}$ and $\partial\bar{\rho}/\partial r$ are then computed. Improved new values of $\overline{Y}$ and $\overline{V}_z$ next can be computed and the iteration repeated until no further change occurs. For the cases investigated, two iterations generally proved sufficient. For the next integration step, the entire procedure is repeated using the newly computed values of $\overline{Y}$ and $\overline{V}_z$ as initial conditions. This procedure was successfully programmed using a variable radial mesh, which greatly reduced computing time [13]. The reasonable agreement between computed and experimental profiles obtained is shown in Table 3.

CONCLUDING REMARKS

Although no attempt was made to solve the energy equation in this investigation because the assumption that the stagnation temperature remained constant appeared valid, the method for solving the simplified turbulent boundary layer energy equation, together with the diffusion and axial momentum equations, again using an iterative procedure was worked out in detail [12, 13]. In this case Pr and Le must be known functions of position as well as E_d, E_m, $\overline{V}_r$ and $\overline{P}$. In addition, either the stagnation enthalpy, or stagnation temperature must be given (or estimated) at the initial axial location as well as the $\overline{Y}$ and $\overline{V}_z$ profiles.

In a combustion chamber the total losses, i.e. total increase in entropy, resulting from injection, shock losses, wall effects and combustion inefficiencies must be minimized; however, the conclusions of this investigation relate only to the mixing. Of course, ultimate injector design for a practical combustor must include all these effects and their interactions.

REFERENCES

1. L. J. ALPINIERI, *AIAA Jl* **2**, 1560 (1964).
2. G. KLEINSTEIN, *J. Spacecraft Rockets* **1**, 403 (1964).
3. P. A. LIBBY, *ARS Jl* **32**, 388 (1962).
4. V. ZAKKAY, E. KRAUSE and S. D. L. WOO, *AIAA Jl* **2**, 1939 (1964).
5. V. ZAKKAY and E. KRAUSE, *Int. J. Heat Mass Transfer* **8**, 1047 (1965).
6. G. N. ABRAMOVICH, *Theory of Turbulent Jets*. M.I.T. Press, Cambridge, Massachusetts (1963).
7. S. I. PAI, *Fluid Dynamics of Jets*. Van Nostrand, New York (1954).
8. J. O. HINZE, *Turbulence*. McGraw-Hill, New York (1959).
9. N. M. HOWE, C. W. SHIPMAN and A. VRANOS, Turbulent mass transfer and rates of combustion in confined turbulent flames, pp. 36–47, *7th Symp. (Int.) Combustion*, Academic Press, New York (1963).
10. A. FERRI, *Jl R. Aeronaut. Soc.* **68**, 575 (1964).
11. W. FORSTALL, JR. and A. H. SHAPIRO, *J. Appl. Mech.* **17**, 399 (1950).
12. J. H. MORGENTHALER, Mixing in supersonic flow, General Applied Science Laboratories, TR 592 (1966).
13. J. H. MORGENTHALER, Supersonic mixing of hydrogen and air, Ph.D. Thesis, University of Maryland (1965).
14. O. LEVENSPIEL, *Chemical Reaction Engineering*. John Wiley, New York (1962).
15. R. F. CLIPPINGER, Supersonic axially symmetric nozzles, Ballistic Research Laboratories, BRL Rept. 794, Aberdeen Proving Ground, Md. (1951).
16. B. S. MASSON, Diffusive separation of a gas mixture approaching a sampling probe, University of California Institute of Engineering Research, Berkeley, California, Series 20, Issue 141 (1962).
17. V. H. REIS and J. B. FENN, *J. Chem. Phys.* **39**, 3240 (1963).
18. L. KINGSLAND, JR., Experimental study of helium and argon diffusion in the wake of a circular cylinder at $M = 5{\cdot}8$, Guggenheim Aeronautical Lab., California Institute of Technology, Hypersonic Research Project Memo 60 (1961).
19. J. P. LONGWELL and M. A. WEISS, *Industr. Engng Chem.* **45**, 667 (1953).

Résumé— Les stratoréacteurs hypersoniques employant la combustion supersonique de l'hydrogène ont des possibilités attrayantes pour l'aviation ou des systèmes de lancement futurs. L'objet de l'étude actuelle était les effets quantitatifs des paramètres d'injection de combustible sur le mélange d'hydrogène gazeux avec un écoulement supersonique d'air à l'intérieur d'une conduite circulaire, afin de fournir quelques bases pour le projet de brûleurs supersoniques de moteurs à performances élevées. L'hydrogène était injecté à une vitesse voisine de celle du son dans des écoulements d'air à un nombre de Mach 2 ou 3, à des rapports globaux équivalents de 0,17 à 0,50, à la fois dans des directions radiales et axiales (vers l'aval) à partir de fentes circonférentielles dans la paroi.

Les résultats montraient que, dans le cas d'une injection radiale, le mélange était considérablement amélioré, bien que la diminution de pression totale était également plus élevée dans ce cas.

La diffusivité massique tourbillonnaire, E_d (coefficient de diffusion turbulent) et la vitesse radiale, $\overline{V}_r$,

étaient déterminées en différentiant les profils de concentration, de vitesse et de masse volumique, obtenus à différentes distances le long de l'axe de l'endroit de l'injection. Pour le cas de l'injection radiale, avec une section d'essai de 25 mm de diamètre intérieur, un modèle simple dans lequel E_d variait seulement dans la direction radiale et $\bar{V}_r$ variait seulement dans la direction axiale, permettait une corrélation raisonnable des résultats expérimentaux. La validité des tendances obtenues pour E_d et $\bar{V}_r$ a été vérifiée par intégration numérique de l'équation de la diffusion, et la solution simultanée des équations de la quantité de mouvement et de la diffusion; les profils calculés sont en accord raisonnable avec les profils expérimentaux aval de concentration et de vitesse. Une méthode de résolution des problèmes de mélange turbulent par une solution simultanée des équations de la diffusion, de la quantité de mouvement et de l'énergie est présentée.

Zusammenfassung—Hypersonische Staustrahlen mit Überschallverbrennung von Wasserstoff weissen attraktive Möglichkeiten für zukünftige Flugzeuge oder Startsysteme auf. Das Ziel der gegenwärtigen Arbeit war, die quantitative Untersuchung von Einflüssen der Parameter der Brennstoffeinspritzung auf die Vermischung des gasförmigen Wasserstoffs mit einem Überschall-Luftstrom in einer zylindrischen Öffnung. Damit sollten grundsätzliche Kenntnisse, die zum Entwurf von Überschall-Brenneinrichtungen für Hochleistungsmaschinen notwendig sind, erworben werden. Wasserstoff von Schallgeschwindigkeit wurde in Luftströme mit Mach 2 und Mach 3, sowohl in radialer als auch achsialer (stromabwärts) Richtung aus Schlitzen am Wandumfang eingeblasen bei Gesamtequivalenzverhältnissen von 0,17 bis 0,50. Die Ergebnisse zeigten, dass beträchtlich bessere Vermischung im Fall radialer Einblasung auftrat, obwohl die Abnahme des Standdruckes in diesem Fall auch grösser war.

Der turbulente Austauschkoeffizient E_d und die Radialgeschwindigkeit $\bar{V}_r$ wurden bestimmt durch Differentation der experimentell in verschiedenen achsialen Abständen von der Einblasstelle gefundenen Konzentrations-, Geschwindigkeits- und Dichteprofile. Im Fall der radialen Einblasung mit einer Messstrecke von 25,4 mm, einem einfachen Modell in dem E_d sich nur in radialer und $\bar{V}_r$ nur in achsialer Richtung änderte, liess sich eine vernünftige Korrelation der experimentellen Ergebnisse finden. Die Gültigkeit der für E_d und $\bar{V}_r$ gefundenen Tendenzen wurde durch numerische Integration der Diffusionsgleichung und gleichzeitiger Lösung der Diffusions- und Bewegungsgleichung nachgeprüft. Die berechneten Profile stimmten ganz gut mit den stromabwärts gefundenen Konzentrations- und Geschwindigkeitsprofilen überein. Eine Methode zur Lösung des turbulenten Mischproblems durch gleichzeitige Lösung der Diffusions- Bewegungs- und Energiegleichung wird angegeben.

Аннотация—Гиперзвуковые летательные аппараты с прямоточным воздушно-реактивным двигателем на водородном топливе весьма перспективны для пусковых установок. Настоящая работа предпринята с целью исследования количественного влияния параметров вдува на перемешивание газообразного водородного топлива со сверхзвуковой струей воздуха, заключенной в цилиндрический канал. Это необходимо для обоснования расчета сверхзвуковых камер мощных двигателей. Водород подавался при звуковой скорости в воздушную струю с числами Маха 2 и 3. Общие отношения компонентов ваьировались в пределах 0,17–0,50. Топливо подавалось через щели по окружности трубы как в радиальном, так и в осевом направлениях. Эксперименты показали, что перемешивание улучшается при радиальной подаче топлива. В этом случае давление торможения заметно снижается.

Коэффициент турбулентного обмена массой Ea и радиальная скорость $\bar{V}_r$ определялись путем дифференцирования полученных из опытов распоеделений концентрации, скорости и плотности, в различных точках по оси от места вдува топлива. Для случая радиального вдува и диаметра трубы 1 дюйм; использовалась простая модель, позволяющая удовлетворительно обобщить экспериментальные данные, в которой Ea изменялась только в радиальном направлении, а $\bar{V}_r$ в осевом. Кривые распределения Ea и $\bar{V}_r$ проверялись численным интегрированием уравнения диффузии и совместным рещением уравнений диффузии и импульса. Расчетные профили удовлетворительно согласуются с экспериментальными распределениями концентрации и скорости.

Предложен метод совместного решения уравнений диффузии, момента и энергии.